Maejo International Journal of Energy and Environmental Communication

Journal homepage: https://ph02.tci-thaijo.org/index.php/MIJEEC

ARTICLE

Research on the electrical characteristics of atmospheric strong ionization dielectric barrier discharge for air pollution control

Prince Junior Asilevi[1,2,*], Daniel Akambawe[2], Chengwu Yu[1], Jue Li[1], Patrick Boakye[3], Sampson Oduro-Kwarteng[2], Muhammad Imran Nawaz[1]

[1]School of Environmental and Safety Engineering, Jiangsu University, Zhenjiang, 212013, Peoples Republic of China
[2]Department of Civil Engineering, Kwame Nkrumah University of Science and Technology, Kumasi, Ghana
[3]Department of Chemical Engineering, Kwame Nkrumah University of Science and Technology, Kumasi, Ghana

ARTICLE INFO

Article history:
Received 19 Feburary 2020
Received in revised form
20 March 2020
Accepted 05 April 2020

Keywords:
Benzene
Strong ionization
DBD
Specific input energy
Current density
Maxwell equation

ABSTRACT

The specific input energy (SIE), current density, and discharge power of homemade strong ionization dielectric barrier discharge (DBD) were studied to suppress gas-phase benzene at atmospheric pressure efficiently. Findings indicate that for 300 ppm of benzene at 3.5 kJ/L SIE, benzene's removal efficiency reached 96%. The decline in current density by 66.48% and 43.7% for an initial benzene concentration of 300 ppm was due to increased oxygen content (from 2.4% to 20.9%) and relative humidity (from 18.9% to 90%), respectively, thus reducing electron concentration and consequentially enhanced the removal efficiency over 93%. Furthermore, the decomposition law's beta parameter decreased from 3.1 kJ/L at 300 ppm to 1.6 kJ/L at 100 ppm, indicating that •O and •OH radicals are key species for the decomposition of benzene and electron dissociation reactions largely control the process. The Maxwell–Boltzmann electron energy distribution function was solved using the average energy of the strong ionization discharge reactor (~10 eV), showing that approximately 84.8 % of high energy electrons possess enough energy to cause the benzene ring cleavage and free radical production. The study results show that the strong ionization DBD plasma reactor is highly efficient in removing benzene from industrial waste air, hence air pollution control.

1. Introduction

Application of non-thermal plasma (NTP) or cold plasma technology for the abatement of volatile organic compounds (VOCs) in industry waste air has become popular as a promising technology adaptable to room temperature and atmospheric pressure. It is highly efficient, energy-saving, and environmentally friendly for the removal of VOCs. High energetic electrons attack gaseous molecules in the plasma system, leading to ionization, splitting of molecules, electronic, vibrational, and rotational excitation of the neutral gas. Electrons, radicals, ions, and excited molecules are the results of these inelastic collisions, consequentially oxidizing O_2, N_2, and H_2O components of the polluted air stream to generate •O and •OH radicals, which further proceed to attack pollutants. Notwithstanding, a few setbacks include low energy efficiency, inferior mineralization efficiency, and the formation of harmful discharge by-products such as ozone (O_3) and NOx (NO and NO_2) (Asilevi et al., 2020; Zhu et al., 2008; Kim et al., 2008).

Dielectric barrier discharge (DBD) is a good NTP source, having low-cost plasma in air pollution control. It has been particularly efficient in removing very low VOCs and odorous

* Corresponding author.
E-mail address: ev_asilevi@yahoo.com (Prince Asilevi Junior)

Nomenclature and abbreviation	
SIE	Specific input energy
NTP	Non-thermal plasma
VOCs	Volatile organic compounds
DBD	Dielectric barrier discharge
GC-MS	Chromatography mass spectrometer
FID	Flame ionization detector

compounds and has added energy-saving and no dioxin production. The strong ionization discharge can be achieved at atmospheric pressure or above atmospheric pressure (Jarraya et al., 2010). In a typical strong ionization DBD, almost all the electronic energy from the applied electric field is transferred to the heavy air molecules, and the electron energy (Te) is calculated from equation (1) as follows (Holzer et al., 2002; Hongxiang et al., 2010):

$$T_e = \frac{\sigma m_h E_g^2}{3kn_e m_e v_e'} \quad (1)$$

where, n_e (cm^{-3}) represents electron concentration, and m_e (eV) and m_h (eV) are the mass of electronic and heavy particles respectively, k, v_e (sec^{-1}), σ (μS/cm), E_g (kV/cm) stand for the Boltzmann constant, electron collision frequency, plasma conductivity, and discharge intensity of the electric field, respectively. Reportedly, during the discharge process, the discharge energy flow density can reach 2.1 W/cm^2, and the average electron energy can exceed 13 eV. Thus the system is classified as strong ionization discharge, which is far higher in energy intensity than other similar dielectric barrier discharge technologies, as shown in Table 1 (Zhang et al., 2017; Son et al., 2017).

Table 1
Main physical parameters of strong ionization discharge and micro-discharge (Adapted from Li et al., 2016).

DBD discharge	Strong ionization discharge	Micro – discharge
Gas pressure	≥0.1 MPa	0.1 MPa
Electric field intensity	100–320 kV/cm	0.1–100 kV/cm
Electron concentration	>1015 cm^{-3}	1014–1015 cm^{-3}
Electron average energy	>10 eV	1–10 eV
Discharge energy	1–2.1 W/cm^2	<1 W/cm^2

DBD: dielectric barrier discharge.

Several researchers have reported VOC decomposition using NTP technology. Karatum and Deshusses (2016) studied the removal efficiency of some common VOCs using DBD reactor under similar experimental conditions (i.e., the gas residence time of 0.016 s and initial concentration of 95–100 ppm). The following removal efficiencies were reported: methyl ethyl ketone (50%), benzene (58%), toluene (74%), 3-pentanone (76%), methyl tert-butyl ether (80%), ethylbenzene (81%), and n-hexane (90%). Different VOCs have different removal efficiencies. Mok and Nam (2002) have noted that plasma generated radicals are the main active species responsible for the decomposition of VOCs in the DBD. Thus oxygen and water vapor may play key roles in the abatement process since they are the main sources of •O and •OH radicals in the plasma system.

Xu et al. (2014) have studied the effect of CuO/AC catalyst with the pulsed corona discharge in enhancing the removal efficiency of benzene. Recently, Liang et al. (2013) also used a ferroelectric catalyst with the DBD to remove toluene. The study underscored the significant role of ozone produced in the plasma in the degradation process, emphasizing the catalyst effect. Zhu et al. (2008) combined the DBD and titanium dioxide photocatalyst in benzene abatement from industry polluted air. Most researchers have focused on improving reactor function largely by the synergistic effect of catalytic metals and photocatalytic technology, although most catalysts have been reported to show poisoning effects.

Again, the DBD device's electrical characteristics' effect drives the decomposition process remains largely nascent in most literature (Mao et al., 2018; Guo et al., 2015; Wu et al., 2017). The aim of this work thus focused on the electrical behavior of the strong ionization DBD to study the mechanism and discharge conditions relevant for the decomposition of benzene, an aromatic and highly volatile carcinogenic VOC. Benzene benumbs the central nervous system and has detrimental effects on human health. Also, it is reportedly the most predominant VOC of the total emissions of hazardous gases from vehicles using conventional gasoline, representing the main source of benzene pollution (Halliday et al., 2016).

Particular attention is paid to the decomposition process's genesis, viz., radical formation, and the main active species available for the radical–pollutant reactions. This is done by studying the current density in the reactor for humid air without the pollutant. Finally, Ozone and NO_x as important byproducts of the strong ionization discharge plasma was studied.

2. Materials and methods

The schematic representation of the whole experimental setup employed in this research presented in Fig. 1.

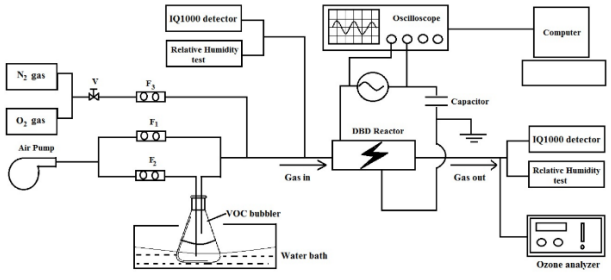

Fig. 1. Schematic of the experimental set-up. V is control valve, while F_1, F_2, and F_3 are the gas mass flow rate meters calibrated in L/min.

The main parts are: (1) the gas flow system comprising the air pump, nitrogen and oxygen gas supply tanks underflow control, (2) the reactor system comprising of the DBD reactor, high voltage AC

supply, and (3) the analytic system comprising of the IQ1000 benzene concentration detector, humidity meter, oscilloscope and computer. The strong ionization discharge reaction volume is 19 cm^3, and the supply voltage frequency is set at 5.883 kHz. The experimental conditions are summarized in table 2.

Table 2
Experimental measurement conditions.

Parameter	Value
Supply frequency	5.883 kHz
Reactor volume	19 cm^3
Benzene concentration	100–400 ppm
Nitrogen flow rate	0.0–1.0 L/min
Relative humidity	15.5–80 %
Voltage	1.0–3.0 kV

2.1. The gas flow system

Nitrogen gas under valve control and air bubbled through the diluted benzene solution prepared at some suitable concentration consistent with the detector limit, placed in a water bath at room temperature. The gaseous mixture then inlets the discharge reactor under varying humidity conditions by changing the water bath temperature. The valve controls the amount of nitrogen gas passing into the reactor. The gas flow rate meters F_1, F_2, and F_3 measure the rates at which the gases flow through the experimental system in L/min.

2.2. The reactor system

Fig. 2 is a schematic view of the strong ionization DBD reactor system used in the experiment. The reactor is a rectangular box, 227 mm × 145 mm × 22 mm in dimension. The sintered metallic silver grounding electrodes are 100 mm × 190 mm, housing a double 1 mm narrow gas gap serving as the discharge reaction chamber. The housing structure is designed to provide a heat sink and an electric fan fixed close to the reactor for cooling during the discharge operation. Across the reactor is a high voltage alternating current power supply to provide the discharge energy.

2.3. The analysis system

The inlet gas is first analyzed before it enters the ionization reactor chamber. This is done using the Model IQ-1000 (International Sensor Technology, California), a portable universal gas detector. The instrument is equipped with the Mega-Gas Sensor, a solid-state sensor designed to detect over 100 toxic and combustible gases.

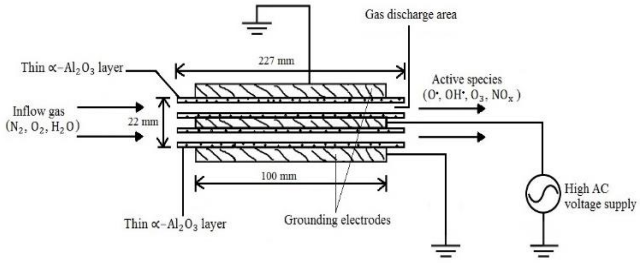

Fig. 2. Schematic representation of the strong ionization DBD reactor.

The calibration is automated and straightforward, with no manual adjustments necessary. The IQ-1000 stores the setup and calibration data for each gas in memory. When gas is selected from the IQ-1000's menu, the IQ-1000 automatically uses the data to conFig. itself properly for the gas selected, allowing the unit to provide an accurate reading of the gas concentration. Power is provided by 6 'D' size alkaline or nickel-cadmium batteries. Finally, the recorded data is displayed on a large backlit LCD screen and then transferred to the computer via an RS-232 port for further analysis. A similar test is repeated for the outlet gas to determine the remnant benzene pollutant's concentration in parts per million (ppm).

The concentration of ozone produced by the DBD at the outlet is detected and measured by the ozone concentration analyzer (CL-7685, B&C electronic, Italy). NO_x concentration is measured by the NOVA5003-S gas analyzer (Tenova, USA). The instrument employs an electrochemical principle to measure the concentration of NO and NO_2. The range of NO is 0–5000 ppm, while NO_2 has a range of 0–800 ppm and a resolution of 1 ppm. A high voltage-time 500 MHz digital oscilloscope (WaveJet 354A) is connected across the high voltage supply to obtain the voltage and charge waveforms. This is done by connecting the high voltage probe (Tektronix, P6015A). The discharge current density is measured with a current probe (Tektronix, TCP303) and the root mean square (RMS) value is analyzed.

The organic byproducts during the decomposition of benzene were determined by Agilent 6890 gas Chromatography (GC) combined with a 5975 mass spectrometer (MS) (Aligent Technologies, CA, USA), fitted with an onboard flame ionization detector (FID) and helium carrier gas (1 mL/ min, constant flow). The sample solution was prepared by dissolving the outlet gas in ethanol and injected into the instrument gas stream using the splitless injection mode. An Agilent DB-5MS (30 m × 0.25 mm × 0.25 µm) capillary column was used for the separation. The column separation tube was set at 170 °C column temperature, 250 °C injection temperature, and 280°C detection temperature. The injection volume of the injector is 10 µL. The initial temperature was set at 40 °C for 3 min, with a heating rate of 10°C / min up to 100 °C， again, 5 °C per minute up to 200 °C, then 10 °C / min up to 300 °C. The total time for the analysis was 38.98 min. Fourier transform infrared spectrum (FT-IR) was taken using the KBr pellet method with the Nicolet Nexus 470 FT-IR

spectrophotometer from Thermo Electron Corporation.

The input charge, *Q*, is obtained by measuring the capacitor voltage in series with the reactor's ground electrodereactor's ground electrode to calculate the input power using the *V*–*Q* Lissajous diagram from the oscilloscope. The entire signal data is processed by the computer connected to the oscilloscope. All calculations and graphical representations were performed on the MATLAB Toolbox Release 2012b, The MathWorks, Inc., Natick, Massachusetts, United States.

2.4 Electrical measurements and calculations

The electricity principally governs VOC decomposition within the plasma system. It is, therefore, of key relevance to quantify the energy released into the system. Thus the following calculations were performed:

Specific input energy (SIE): This is the energy used within the reactor for the decomposition process by a unit volume of polluted gas (Wu et al., 2017). It is calculated as:

$$SIE = 60P/F \quad (2)$$

Where *P* is the high voltage input power and *F* is the gas flow speed measured in L/ min.

Degree of removal (C_{out}/ C_{in}): This is the ratio of final VOC concentration after degradation to initial VOC concentration. For a particular VOC pollutant, the removal degree is dependent on the SIE and an input energy parameter called β (beta-parameter) according to equation (2).

$$C_{out} = C_{in} \exp(SIE/\beta) \quad (3)$$

where C_{in} and C_{out} are the initial and output benzene concentrations, and β is the specific energy constant. The degree of removal reduces as more pollutant is removed and hence the removal efficiency can be obtained as $1 - (C_{out}/C_{in})$ (Rosocha, 2005).

Discharge power (P): The average electrical power in watts (W) deposited into and consumed by the plasma ionization reactor chamber. This is needed to calculate the SIE and to characterize the decomposition energy consumption. This paper follows the *Q*–*V* Lissajous curve method for calculating discharge power, first reported by Manley (1943) and recently shown by a host of researchers to give possible energy studies results in DBD plasma reactor studies (Kriegseis et al., 2011). It is given as

$$P = \frac{1}{T}\int_0^T V_r(t).C_m\frac{dV_m(t)}{dt}dt = \frac{1}{T}\int V_r C_m dV_m = \frac{1}{T}\oint V_r\, dQ_m \quad (4)$$

Where *T* is the AC cycle period, V_r is the high voltage across the reactor, and C_m is the capacitance of the series capacitor, also called monitor capacitor. A large capacitance must be chosen relative to the reactor capacitance to ensure a very small voltage (V_m) across it. Q_m is the charge on the capacitor. In the experiment, a 4.7 μF capacitor is chosen (see Fig. 1). The small voltage drop (V_m) across the series capacitor is measured with the MASTECH MY-65 digital multimeter, entered into a MATLAB code to compute the charge, Q_m.

A graph of Q_m against V_r displayed on the oscilloscope is usually a parallelogram, called the Lissajous curve, whose area is the energy deposited within the reactor. Thus equation (3) can finally be written as:

$$P = f \times A \quad (5)$$

where *f* is the high voltage AC frequency in Hertz and *A* is the Lissajous area. The digital oscilloscope measures the electric signals.

3. Results and discussion

3.1. Energy characteristics of strong ionization DBD

In order to discuss the efficient decomposition of benzene, the ionization energy deposited within the DBD reactor is an indispensable parameter. This paper uses the *Q*–*V* Lissajous method to obtain power deposited into the DBD. The Lissajous curve has a parallelogram shape whose area equals the energy deposited (Kriegseis et al., 2011). The typical voltage and current waveforms of the strong ionization DBD displayed on the oscilloscope are shown in Fig. 3. The applied voltage amplitude is 3.5 kV, with the corresponding current waveform showing several short peaks indicating micro discharge activity in the DBD plasma. Each pulse correlates with a series of micro discharges.

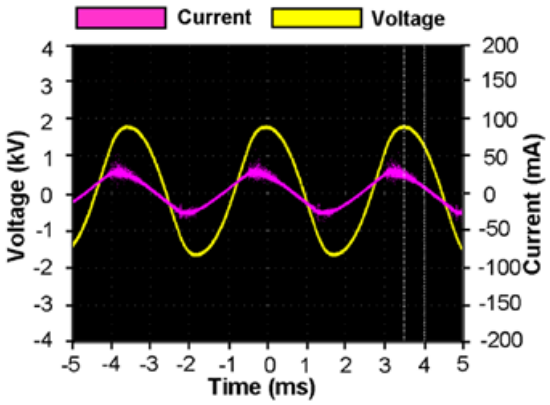

Fig. 3. Typical voltage and current waveforms of strong ionization dielectric barrier discharge in air are displayed on the oscilloscope.

Fig. 4. represents the *Q*–*V* Lissajous diagram displayed on the oscilloscope screen for two different applied voltages (3.5 kV and 2 kV). The power calculated for the larger and smaller Lissajous areas is 5.49 W and 0.33 W, respectively. This means more energy is deposited at higher voltages and thus, ionization is expected to be greater with increasing energetic electrons and consequentially enhancing removal efficiency. Rosocha (2005) showed that the degree of removal (C_{out}/C_{in}) of VOC pollutants reduces as more pollutant is destroyed and depends on the SIE and a characteristic energy-density parameter (β) which is specific to the target pollutant, the background gas, and the reduced electric field for the discharge reactor (Kriegseis et al., 2011).

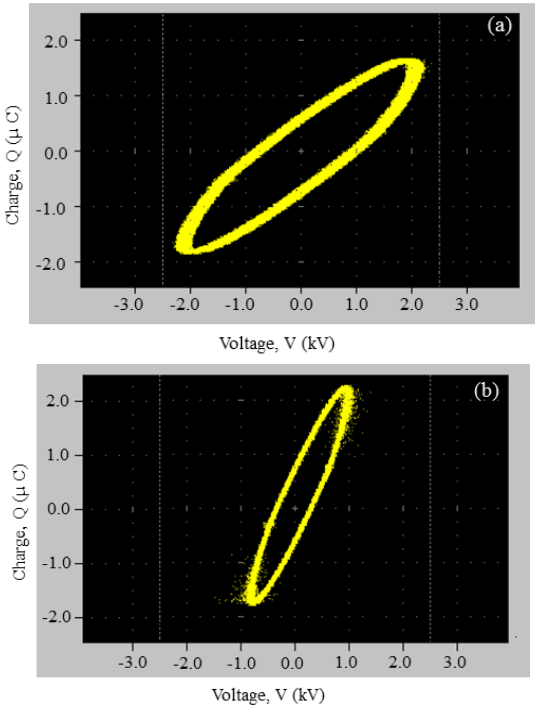

Fig. 4. *Q–V* Lissajous Fig. at 1 mm discharge gap and 6 kHz frequency in air. (a) 3.5 kV voltage supply and (b) 2 kV voltage supply

Theoretically, the physical structure of the strong ionization DBD equipment illustrated in Fig. 5 is akin to a lossy capacitor pair comprising of discharge electrodes, a dielectric layer and a thin discharge gap, which can be compared to a resistive, capacitive load (Fig. 5a). The entire circuit is equivalent to a series resonance, and the voltage at the reactor terminals can be many times larger than the average voltage. When the polarization intensity of the dielectric bathed in a uniform electrostatic field is high enough, many charges accumulate at the tip of its surface, which will produce an increased local inhomogeneous electric field. The intensity of the electric field is shown in equation 6 (Zhu et al., 2008; Böhm et al., 2016):

$$E = (3\varepsilon/ \varepsilon + 2)\, Eo \cos\theta \quad (6)$$

Where E is the local electric field strength, ε is the permittivity, and θ is the phase angle between the current and the voltage.

It can be ascertained that the quantity of E is proportional to E_0, and the larger the dielectric constant, the closer E becomes three times of E_0 at θ = 0. Therefore, increasing average voltage creates higher electric field strength, enhancing discharge power. Thus, high-energy electrons generated by burgeoning discharge power create pulses increasing the probability of collision with benzene molecules, thus enhancing removal efficiency. Fig. 5b and the following experimental evaluations validate this theory. It was realized that discharge power is greatly enhanced by 63.9% for increasing supply voltage at 5.8 kHz. This is in tandem with the report by Bo et al. (2007), Liang et al. (2015), and Boucher and Katz (1967).

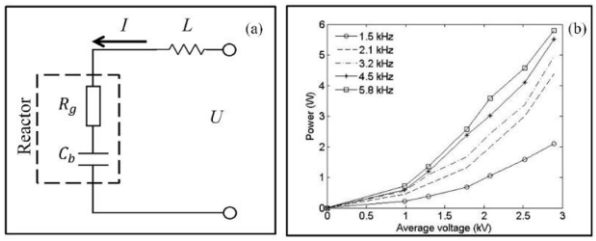

Fig. 5. (a) Reactor equivalent capacitive circuit, and (b) effect of average voltage supply on discharge power.

In this regard, Qian et al. (2018) and Bo et al. (2007) have shown that the degree of removal (Cout/Cin) of VOC pollutants reduces as more pollutant is destroyed and depends on the SIE and a characteristic energy-density parameter (β) which is specific to the target organic pollutant, the background gas, and the reduced electric field for the discharge reactor.

Fig. 6. shows a graphical representation of the physical implication of equation (2). The impact of reactor input energy density on benzene decomposition is studied for three initial concentrations (300, 150, 100 ppm). It is noticed that the degree of removal ([C_{out} /C_{in}]) is an exponential decay function of the input energy. This means that increasing discharge energy deposited into the reactor will increase ionization and increase the benzene pollutant's decomposition, thereby decreasing the remaining concentration. The degree of removal of benzene pollutants, is thus expected to reduce as SIE rises, accounting for a percentage increase in removal efficiency.

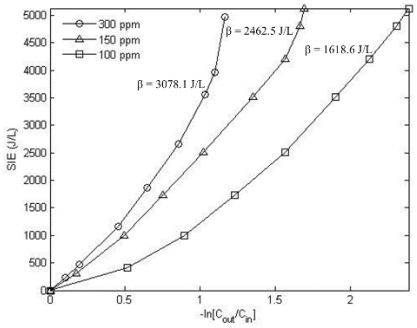

Fig. 6. Degree of removal plot showing the exponential decay relation with SIE at different initial benzene concentrations (200, 150, 100 ppm) in air.

It is also seen that at 100 ppm of initial benzene concentration, the degree of removal is between 0.59 and 0.09, while at 300 ppm of initial benzene concentrations, the degree of removal is between 0.90 and 0.31. Consequentially, the removal efficiency will be more significant for the lower initial benzene concentration, as other researchers affirmed. Fig. 6. further shows the evolution of the beta parameter, β, in equation (3). β decreases from 3078.1 J/L at 300 ppm to 1618.6 J/L at 100 ppm. The beta parameter correlates linearly with the initial VOC concentration, and its corresponding decrease with lower concentrations at ambient temperature is

affirmed in the literature (Qian et al., 2018). The parameter is a VOC specific energy index characterizing decomposition energy demand for the particular VOC by reducing the concentration by the factor of 1/e. It is thus evident that energy demand is higher for increased initial concentration and vice-versa.

3.2 Active species for decomposition reaction process

The decomposition of benzene in the strong ionization discharge reactor is initiated and enhanced by free radicals that serve as active species in the reactor chamber. Key active species are •O and •OH radicals generated primarily from the breakdown of oxygen gas and water vapor (Ye et al., 2008; Sun et al., 1997). This section investigates the formation of the •O and •OH radicals and their role in controlling the initial decomposition process of benzene by studying the impact of gaseous oxygen and water vapor on the current density, removal efficiency, and the energy yield of the reactor.

Fig. 7. shows that for a consistent increase in supply voltage, the current density significantly reduces as the amount of oxygen concentration by percent volume increases. Similarly, Fig. 7. shows that current density decreases under increasing relative humidity (RH) conditions (RH less than 60%).

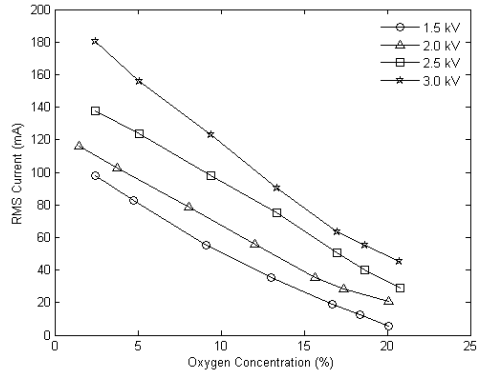

Fig. 7. Impact of percent oxygen concentration by volume on the current density (electron availability) for 300 ppm benzene in air plus nitrogen (to reduce oxygen concentration).

The observation shows that water vapor and oxygen gas have a reducing effect on the discharge current density hence electron density. This is because electrons produced by the discharge process are consumed to breakdown O_2 gas and H_2O vapor to produce •O and •OH radicals, respectively. This, in turn, reduces the amount of conducting electrons hence current density. What's more, it has been reported in the literature that these species have strong oxidation potential, electron affinity, and low bond strength (5.1 eV for O–O) (Mok and Nam, 2002). This is the source of free radicals for the initial decomposition of benzene. The key process involved is reported in table 2 (Bo et al., 2007). Equations 7 – 10 show the ionization and dissociation processes of oxygen molecules in the gas stream, leading to many active particles such as excited oxygen molecules and active oxygen molecules. The reaction products O_2^+ ($X^2\pi g$) and O_2^+ ($A^4\pi g$) are ionized oxygen molecules that are both unstable and continue to dissociate into O (^3P), O (^2D) and other oxygen ions. The generated O (^3P) and O (^2D) are active oxygen atoms, where O (3P) is an oxygen radical •O. Equations 11 and 12 show the ionization reaction of nitrogen molecules, which is also the main reaction that produces secondary electrons.

Equations 13 and 14 are the dissociation reaction of nitrogen molecules, which generate corresponding free radical atoms. It is worth mentioning that, in practice, the entire chemical reaction processes generated within the plasma system in the strong ionization discharge are a more complicated set of reactions. The listed reactions show only the secondary electrons and the major free radicals generated when the discharge occurs in the air stream. In addition, •OH, O_3 and other active particles are also generated by inelastic collisions between high-energy electrons and O_2 and H_2O molecules (Asilevi et al., 2020). Oxygen (O_2) gas and water (H_2O) vapor are key airstream components driving plasma discharge strength and hence the decomposition reaction pathway of benzene can easily be controlled.

Table 2
Key ionization reactions in the strong ionization DBD

Reaction process	K, reaction rate (cm^3/s)	Equation numbers
$e^- + O_2 \rightarrow O_2^+X^2\pi_g + 2e^-$	4.2×10^{-11}	(7)
$e^- + O_2 \rightarrow O_2^+A^4\pi_g + 2e^-$	9.1×10^{-13}	(8)
$e^- + O_2 \rightarrow O\ (^3P) + O\ (^2D)\ e^-$	4.6×10^{-16}	(9)
$e^- + O_2 \rightarrow O\ (^3P) + O\ (^1D)\ e^-$	3.2×10^{-11}	(10)
$e^- + N_2 \rightarrow N_2^+(X^2\Sigma_g^+) + 2e^-$	1.1×10^{-10}	(11)
$e^- + N_2 \rightarrow N_2^+(B^2\Sigma_u^+) + e^-$	2.7×10^{-11}	(12)
$e^- + N_2 \rightarrow N\ (^4S) + N\ (^4D) + e^-$	2.4×10^{-17}	(13)
$e^- + N_2 \rightarrow N\ (^4S) + N\ (^2D) + e^-$	2.0×10^{-11}	(14)
$e^- + H_2O \rightarrow e^- + H + OH$	2.6×10^{-12}	(15)
$e^- + H_2O \rightarrow 2\ e^- + H_2^+$	1.1×10^{-12}	(16)

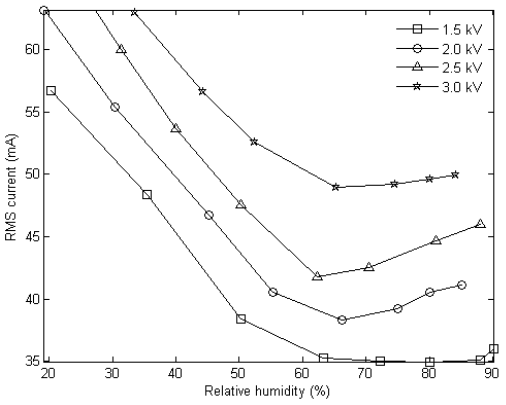

Fig. 8. Impact of relative humidity (RH) on the current density (electron availability) for 300 ppm benzene in air.

However, Fig. 8 shows that water vapor only reduces discharge current within some stipulated limit (50%–70%), beyond which its effect is insufficient. This may result from a complete change in the entire plasma system due to excess water vapor reducing the effective transfer of charge within the plasma system's micro discharge. Thus, it is reported that the removal efficiency of VOC

in DBD plasma significantly reduces after some RH limit (Ma et al., 2016).

The decomposition efficiency of benzene was enhanced by increasing oxygen concentration by volume and increasing water vapor (RH). This indicates that the benzene was effectively decomposed by producing the active species in the strong ionization DBD reactor. The amount of energy deposited into the reactor, SIE in J/L is also correlated with the removal efficiency.

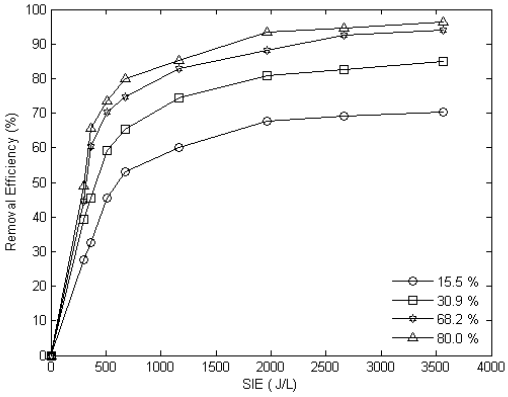

Fig. 9. Impact of SIE on removal efficiency concerning RH (15.5%, 30.9%, 68.2%, and 80%) for 300 ppm initial benzene concentration in air.

Fig. 9 shows the impact of water vapor on benzene removal efficiency in the strong ionization DBD for 300 ppm of benzene at 15.5%, 30.9%, 68.2%, and 80% RH. Efficiency of removal at 0.5 kJ/L is 45.5%, 59.1%, 70.4%, and 73.7% respectively, and for a relatively higher SIE of 3.5 kJ/L it is 70.4%, 84.9%, 93.9%, and 96.2% respectively. The evolution of removal efficiency is enhanced by appreciably more humid air, notwithstanding the insignificance at closely higher RH. Future study will investigate temperature and ozone effects since temperature relates linearly with molecular energy and ozone is reportedly an important gaseous product of air plasma ionization (Khan and Ghoshal, 2000). When the oxygen volume concentration increased from 3.7% to 8.7% the decomposition efficiency was enhanced by 57.68%.

3.3 Effect of initial Benzene concentration

Fig. 10 shows the impact of initial benzene concentration on pollutant removal with respect to oxygen concentration. The initial concentration is varied in the range of 50–390 ppm with a total gas flow rate of 10 L/ min and a supply voltage of 2.8 kV. The efficient removal of benzene pollutants is significantly dependent on the initial concentration of benzene and the amount of oxygen content in the flowing air. This is shown by the decreasing trend in the removal efficiency as the initial concentration increases. For example, the removal efficiency is 88% at an initial concentration of 50 ppm but decreases to 70% as the initial concentration increases to 350 ppm, for ambient air conditions. For a given processed stream, the amount of reactive species, high-energy electrons and active species generated by plasma could be the same at certain specific operating conditions. Increasing the inlet concentration of benzene will increase the number of benzene molecules flowing into the reactor. That is to say, each benzene molecule shares less active species and electrons, leading to a reduction of significant benzene removal efficiency (Khan and Ghoshal, 2000).

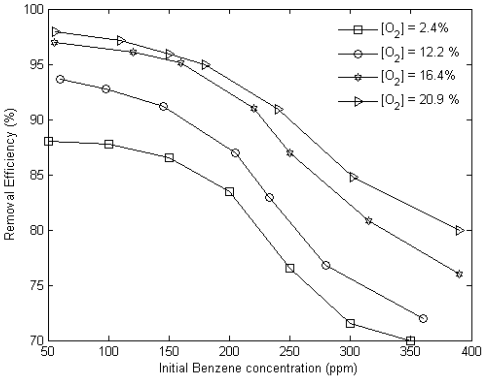

Fig. 10. Impact of initial benzene concentration on benzene decomposition efficiency for different oxygen content conditions, at 2.8 kV and a total airflow rate of 4 L/ min.

3.4 Production of ozone (O_3)

Fig. 11 shows the variation of ozone produced by the strong ionization DBD with SIE under different initial concentrations of the benzene pollutant. It is noticed that ozone production is highest (5.5 mg/ L) at SIE of 3.56 kJ/L when no benzene is present and lower (0.8 mg/ L) at SIE of 4.16 kJ/L when benzene concentration is 100 ppm.

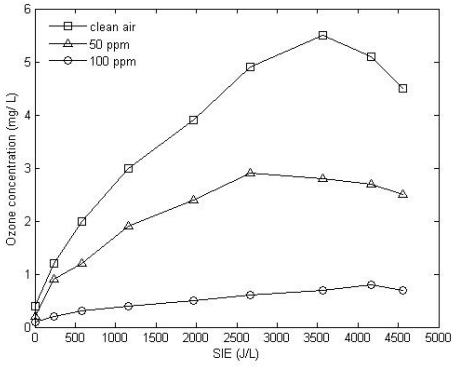

Fig. 11. Ozone formation under varying SIE for oxygenated clean air, 50 ppm, and 100 ppm of benzene in air and oxygen gas, and 4 L/ min flow rate.

The presence of benzene pollutants suppressed the production of ozone. This is consistent with the observation of Jiang et al., 2013 and Karatum and Deshusses (2016) and is reportedly the result of ozone consumption during VOCs' oxidative degradation in the DBD.

Another significant observation is the sharp decline of ozone production after a maximum is reached for all three cases. This has been attributed to the rising temperature and increased electron

density in the discharge reactor as SIE increases, resulting in the quick breakdown of ozone (Liang et al., 2013; Yao et al., 2015).

3.5 Production of NOx

NO_x is an important byproduct of the DBD reactor, predominantly resulting from nitrogen in the air used as carrier gas (Xu et al., 2014). Fig. 12 shows the main NO_x species (NO and NO_2), detected at ambient temperature (27 ºC) and atmospheric pressure. For the SIE range of 239.2–4162.1 J/L, the concentration range of NO and NO_2 is 3.58–10.92 mg/m3 and 19.22–40.59 mg/m3. The concentrations of the two main NO_x species (NO and NO_2) increases with increasing SIE, while the concentration range of NO is lower than NO_2. This is attributed to the presence of ozone and other active species (•O and •OH) generated by the discharge reactor, which quickly oxidizes NO. Yu-fang et al. (2006) have shown a series of possible reactions leading to NOx species' formation and oxidation during a DBD – catalyst process.

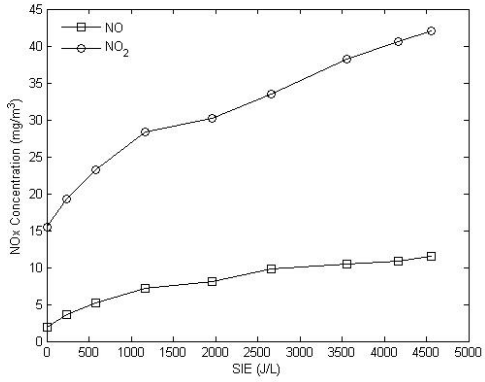

Fig. 12. NO_x formation under varying SIE at 100 ppm benzene and 4 L/ min flow rate in air.

3.6 Decomposition mechanism of benzene

3.6.1 Benzene cleavage and electron energy

In order to understand the breakdown of benzene in our strong ionization plasma, it is important to account for the role of energetic electrons within the ionization discharge chamber, hence the amount of benzene consumed and byproduct formation. According to Ye et al. (2008) the energy of electrons available within the reactor chamber widely varies and thus follows a Maxwellian distribution function shown in equation (17) below:

$$f(\varepsilon) = 2.07 \times \left(10^{-3/2}\right)\varepsilon^{1/2} e^{-1.5\varepsilon/\bar{\varepsilon}} \quad (17)$$

Since the average kinetic energy of electrons in the strong ionization DBD is ~ 10 eV, by replacing $\bar{\varepsilon}$, Eq. 17 becomes:

$$f(\varepsilon) = 2.07 \times \left(10^{-3/2}\right)\varepsilon^{1/2} e^{-15\varepsilon/10} = 0.0655\varepsilon^{1/2} e^{-0.15\varepsilon} \quad (18)$$

After a series of complex mathematical operations, the percentage of electrons E(a) can be calculated by:

$$E(a) = 0.0655 \times \left[\sqrt{0.15a}/_{2e^{-0.15a}} + 17.21e^{-0.15a}\left(\sqrt{0.15a} + 1.57\right)\right] \quad (19)$$

E(a) is the percent amount of electrons possessing the minimum energy required for bond cleavage in the above equation. The term ε is the average energy of electrons in the plasma ionization reactor.

Benzene is a very stable hydrocarbon composed of six carbon atoms joined in a ring with one hydrogen atom attached to each. Cleavage of the benzene ring requires about 5.4 eV. Since the average energy of electrons in the strong ionization discharge reactor is ~10 eV, by solving equation (17), we obtain approximately 84.8% of electrons possessing the minimum energy required to cause cleavage in benzene. This means that more than half of electron – benzene collision can effectively result in a complete breakdown producing CO_2 and H_2O directly. Meanwhile, not all energetic electrons will proceed to initial benzene cleavage, some accounting for equations (7) to (16) resulting in the production of •O and •OH radicals. This may be responsible for the appreciably high decomposition efficiencies reaching 90% and beyond realized in this experiment. Hongxiang et al. (2010) have shown that removal efficiencies in strong ionization discharge can exceed 93% (almost complete VOC abatement).

3.6.2 Benzene cleavage byproducts

Fig. 13 shows the GC-MS display of the gaseous byproducts at the outlet resulting from the decomposition of benzene by the strong ionization DBD. It is apparent that some organic compounds resulting from the decomposition of benzene have been detected. The high electron energy (~10 eV) and the high free radical reactivity in the strong ionization plasma reactor affords high removal efficiency.

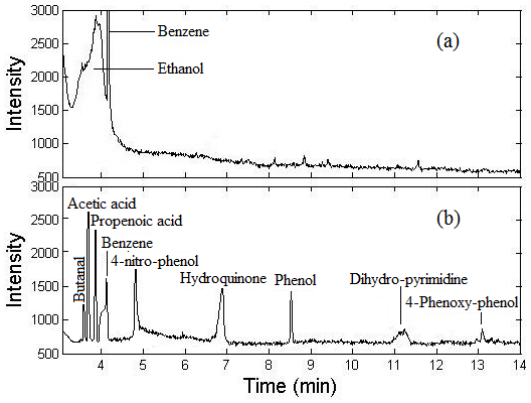

Fig. 13. GC–MS diagram of organic byproducts in the outlet gas at ambient temperature and 300 ppm initial concentration: (a) inlet gas and (b) outlet gas after plasma treatment.

Fig. 13(a) shows the preliminary chromatographic result for the outlet gas at 300 ppm benzene concentration before the discharge process. Two large peaks representing ethanol and benzene at peak

intensities of 2855 and 7195, respectively, were detected. This is expected since the gaseous benzene in the synthetic polluted air was collected in ethanol. Fig. 13(b) displays the outlet gas chromatogram at 300 ppm benzene and 2.5 kV. After the collision of high energy electrons with benzene to form phenyl (C_6H_5) radical, a series of addition and substitution reactions continue with •O and •OH radicals, along with NO_2 (formed possibly by equation (11)) leading to the formation of 4-nitro-phenol ($C_6H_5NO_3$), hydroquinone, and phenol (C_6H_5OH), at peak intensities of 1750, 1500, and 1389 respectively.

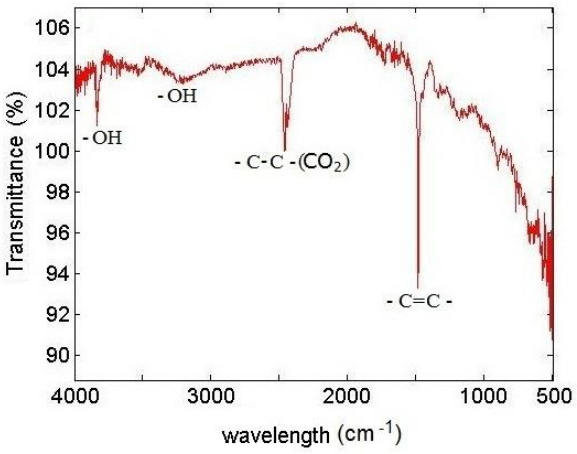

Fig. 14. FTIR spectrum of the products from decomposition of benzene in strong ionization DBD at ambient temperature, 300 ppm initial concentration, 1.5 kV, and 4 L/ min flow rate in air.

Some aliphatic compounds such as acetic acid, propenoic acid, and butanal were also detected between 3 and 4 min along with other peaks such as hydro-pyrimidine and 4-phenoxy-phenol. Some other fine peaks are also shown in the chromatogram, but their respective spectral resolutions are insignificant. High energy electrons may further attack these aromatic compounds, leading to ring cleavage. These organic compounds are similar to other researchers' results using low voltage DBD operation (Liang et al., 2015; Wang et al., 2017; Jiang et al., 2013; Boucher and Katz, 1967).

The implication is that benzene decomposition in the strong ionization DBD with the •O and •OH radicals is an environmentally clean technology. Fig. 14 shows the emission spectra analysis of the byproducts of benzene decomposition using the FTIR (Fourier Transform Infrared Spectrum) for 300 ppm benzene concentration. The spectrum shows C=C stretching frequency around 1500 cm^{-1} in the fingerprint region. A sharp stretch at 2500 cm^{-1} is indicative of a C-C peak. This peak could also represent the presence of CO_2. Present in the IR spectrum is weak broadband at 3300 cm^{-1} signifying the presence of –OH. Another sharp and strong peak in the functional group region was observed at 3700 cm^{-1}. This further shows–OH (Xu et al., 2014; Boucher and Katz, 1967).

4. Conclusion

This study has achieved a good working knowledge of the electrical mechanism and reactor discharge conditions necessary for the efficient removal of benzene using the strong ionization dielectric barrier discharge reactor at atmospheric pressure. In the experiment, the current probe (Tektronix, TCP2020) connected to the high voltage-time 500 MHz Digital Oscilloscope (WaveJet 354A) was used to monitor the current density in the reactor when the oxygen content and water vapor is changing. ~35.5% increase in oxygen content and relative humidity (from 18.9% to 84.1%) reduced the current density by 66.48% and 43.7%, respectively. This is accounted for as the result of electron consumption in the breakdown of air molecules such as O_2, N_2 and H_2O, leading to free active radicals such as •O and •OH. Concurrently, the removal efficiency of the benzene is observed to increase. Thus, it is apparent that the •O and •OH radicals must be key factors controlling the overall breakdown of benzene in the plasma reactor. Meanwhile, the Maxwell-Boltzmann electron energy distribution function also showed that approximately 84.8% of the high energy electrons possess enough energy to cause benzene ring cleavage and free radical production, fitly accounting for the high removal efficiencies realized. Further, the GCMS and FTIR test results revealed that the main decomposition byproducts were 4-nitro-phenol ($C_6H_5NO_3$), hydroquinone, and phenol. Overall, benzene removal from polluted air can be appreciably attained at high efficiencies using the strong ionization DBD other than the low electron energy type technology.

Declaration of competing interest

The authors declare that they have no known competing financial interests or personal relationships that could have influenced the work reported in this paper.

Acknowledgments

This work is supported by the Zhenjiang City Key R&D Project for Social Development (SH2017056).

References

Asilevi, P. J., Yi, C. W., Li, J., Nawaz, M. I., Wang, H. J., Yin, L., & Junli, Z. 2020. Decomposition of formaldehyde in strong ionization non-thermal plasma at atmospheric pressure. International Journal of Environmental Science and Technology 17(2), 765-776.

Böhm, P., Kettlitz, M., Brandenburg, R., Höft, H., & Czarnetzki, U. 2016. Determination of the electric field strength of filamentary DBDs by CARS-based four-wave mixing. Plasma Sources Science and Technology *25*(5), 054002.

Bo, Z., Yan, J. H., Li, X. D., Chi, Y., Cen, K. F., & Cheron, B. G. 2007. Effects of oxygen and water vapor on volatile organic compounds decomposition using gliding arc gas discharge. Plasma Chemistry and Plasma Processing 27(5), 546-558.

Boucher, L. J., & Katz, J. J. 1967. The infared spectra of metalloporphyrins (4000-160 cm^{-1}). Journal of the American Chemical Society 89(6), 1340-1345.

Guo, Y., Liao, X., Fu, M., Huang, H., & Ye, D. 2015. Toluene decomposition performance and NOx by-product formation during DBD-catalyst process. Journal of Environmental Sciences 28, 187-194.

Halliday, H. S., Thompson, A. M., Wisthaler, A., Blake, D. R., Hornbrook, R. S., Mikoviny, T.,. & Hills, A. J. 2016. Atmospheric benzene observations from oil and gas production in the Denver-Julesburg Basin in July and August 2014. Journal of Geophysical Research: Atmospheres 121(18), 11-055.

Holzer, F., Roland, U., & Kopinke, F. D. 2002. Combination of non -thermal plasma and heterogeneous catalysis for oxidation of volatile organic compounds: Part 1. Accessibility of the intra -particle volume. Applied Catalysis B: Environmental 38(3), 163-181.

Hongxiang, O., Chengwu, Y., Wenming, Q., Songmei, W., Qianqian, L., Jing, C., & Li, M. (2010, June). Study on formaldehyde degradation using strong ionization discharge. In 2010 international conference on mechanic automation and control engineering (pp. 2094-2097). IEEE.

Jarraya, I., Fourmentin, S., Benzina, M., & Bouaziz, S. 2010. VOC adsorption on raw and modified clay materials. Chemical Geology 275(1-2), 1-8.

Jiang, N., Lu, N., Shang, K., Li, J., & Wu, Y. 2013. Effects of electrode geometry on the performance of dielectric barrier/packed-bed discharge plasmas in benzene degradation. Journal of hazardous materials 262, 387-393.

Karatum, O., & Deshusses, M. A. 2016. A comparative study of dilute VOCs treatment in a non-thermal plasma reactor. Chemical Engineering Journal 294, 308-315.

Kriegseis, J., Möller, B., Grundmann, S., & Tropea, C. 2011. Capacitance and power consumption quantification of dielectric barrier discharge (DBD) plasma actuators. Journal of Electrostatics 69(4), 302-312.

Khan, F. I., & Ghoshal, A. K. 2000. Removal of volatile organic compounds from polluted air. Journal of loss prevention in the process industries 13(6), 527-545.

Kim, H. H., Ogata, A., & Futamura, S. 2008. Oxygen partial pressure-dependent behavior of various catalysts for the total oxidation of VOCs using cycled system of adsorption and oxygen plasma. Applied Catalysis B: Environmental 79(4), 356 -367.

Liang, W. J., Ma, L., Liu, H., & Li, J. 2013. Toluene degradation by non-thermal plasma combined with a ferroelectric catalyst. Chemosphere 92(10), 1390-1395.

Liang, P., Jiang, W., Zhang, L., Wu, J., Zhang, J., & Yang, D. 2015. Experimental studies of removing typical VOCs by dielectric barrier discharge reactor of different sizes. Process Safety and Environmental Protection 94, 380-384.

Ma T, Jiang H, Liu J, Zhong F. 2016. Decomposition of Benzene Using a Pulse-Modulated DBD Plasma. Plasma Chemistry and Plasma Processing 36(6): 1533-1543.

Manley, T. C. 1943. The electric characteristics of the ozonator discharge. Transactions of the electrochemical society 84(1), 83.

Mao, L., Chen, Z., Wu, X., Tang, X., Yao, S., Zhang, X., & Nozaki, T. 2018. Plasma-catalyst hybrid reactor with CeO2/γ-Al_2O_3 for benzene decomposition with synergetic effect and nano particle by-product reduction. Journal of Hazardous Materials, 347, 150-159.

Mok, Y. S., & Nam, I. S. 2002. Modeling of pulsed corona discharge process for the removal of nitric oxide and sulfur dioxide. Chemical Engineering Journal 85(1), 87-97.

Qian, W. A. N. G., Feng, L. I. U., Chuanrun, M. I. A. O., Bing, Y. A. N., & Zhi, F. A. N. G. 2018. Investigation on discharge characteristics of a coaxial dielectric barrier discharge reactor driven by AC and ns power sources. Plasma Science and Technology 20(3), 035404.

Rosocha, L. A. 2005. Nonthermal plasma applications to the environment: gaseous electronics and power conditioning. IEEE Transactions on Plasma Science 33(1), 129-137.

Son, Y. S. 2017. Decomposition of VOCs and odorous compounds by radiolysis: A critical review. Chemical Engineering Journal 316, 609-622.

Sun, B., Sato, M., & Clements, J. S. 1997. Optical study of active species produced by a pulsed streamer corona discharge in water. Journal of Electrostatics 39(3), 189-202.

Wang, B., Chi, C., Xu, M., Wang, C., & Meng, D. (2017). Plasma -catalytic removal of toluene over CeO2-MnOx catalysts in an atmosphere dielectric barrier discharge. Chemical Engineering Journal 322, 679-692.

Wu, A., Li, X., Yan, J., Yang, J., Du, C., Zhu, F., & Qian, J. 2017. Co-generation of hydrogen and carbon aerosol from coalbed methane surrogate using rotating gliding arc plasma. Applied Energy 195, 67-79.

Xu, N., Fu, W., He, C., Cao, L., Liu, X., Zhao, J., & Pan, H. 2014. enzene removal using non-thermal plasma with CuO/AC catalyst: reaction condition optimization and decomposition mechanism. Plasma Chemistry and Plasma Processing 34(6), 1387-1402.

Yao, S., Wu, Z., Han, J., Tang, X., Jiang, B., Lu, H., ... & Kodama, S. (2015). Study of ozone generation in an atmospheric dielectric barrier discharge reactor. Journal of Electrostatics 75, 35-42.

Ye, Z., Zhang, Y., Li, P., Yang, L., Zhang, R., & Hou, H. 2008. Feasibility of destruction of gaseous benzene with dielectric barrier discharge. Journal of Hazardous materials 156(1-3), 356 -364.

Yu-fang, G., Dai-qi, Y., Ya-feng, T., & Ke-fu, C. (2006). Humidity effect on toluene decomposition in a wire-plate dielectric barrier discharge reactor. Plasma Chemistry and Plasma Processing 26(3), 237-249.

Zhang, H., Fengsen, Z. H. U., Xiaodong, L. I., & Changming, D. U. 2017. Dynamic behavior of a rotating gliding arc plasma in nitrogen: effects of gas flow rate and operating current. Plasma Science and Technology 19(4), 045401.

Zhu, T., Li, J., Jin, Y. Q., Liang, Y., & Ma, G. 2008. Decomposition of benzene by non-thermal plasma processing: Photocatalyst and ozone effect. International Journal of Environmental Science & Technology 5(3), 375-384.